Selective Optical Generation of Coherent Acoustic Nanocavity Modes

M. F. Pascual Winter,[1,2] G. Rozas,[1] A. Fainstein,[1,*] B. Jusserand,[2] B. Perrin,[2] A. Huynh,[2] P. O. Vaccaro,[3,†] and S. Saravanan[3]

[1]*Centro Atómico Bariloche and Instituto Balseiro, C.N.E.A., 8400 S. C. de Bariloche, R.N., Argentina*
[2]*Institut des Nanosciences de Paris, CNRS, Universités Paris 6 et 7, Campus Boucicaut, 140 Rue de Lourmel, 75015 Paris, France*
[3]*ATR Wave Engineering Laboratories, 2-2-2 Hikaridai, Keihanna Science City, Kyoto 619-0288, Japan*

(Received 30 January 2007; published 28 June 2007)

Femtosecond pump-probe experiments on a $Ga_{0.85}In_{0.15}As$ nanocavity enclosed by two $Ga_{0.85}In_{0.15}As/AlAs$ phonon Bragg mirrors reveal selective generation of terahertz confined acoustic modes and regular folded phonons. Selective generation of the confined modes alone is achievable for laser excitation at certain energies below the mirror absorption edges, corresponding to electronic transitions within the cavity layer only. Calculations based on the photoelastic effect explain the experimental results. Decay times of cavity and regular modes evidence longer decay times and anharmonic effects for the cavity mode.

DOI: 10.1103/PhysRevLett.98.265501 PACS numbers: 63.22.+m, 43.38.+n, 78.47.+p, 78.67.Pt

Acoustic nanocavities opened the possibility of confinement and amplification of acoustic phonons in the megahertz-terahertz range [1]. They are interesting in the development of coherent monochromatic acoustic sources and as feedback systems for sound amplification by stimulated emission of radiation. Experiments on the coherent control of acoustic phonons have shown attractive potentialities [2], particularly if performed on monochromatic oscillations. Important progress has been recently achieved in the search for monochromatic sources. Emission of terahertz phonons in superlattice nanostructures under vertical electron transport has been reported [3]. Furthermore, phonon propagation through a nanocavity has been studied by means of transmission experiments by picosecond acoustics where broadband phonon generation is attained by strong light absorption in an aluminum cap layer [4]. In the present work, we provide a method for *selective* optical excitation of coherent nanocavity modes by direct generation in the heterostructure. Direct generation presents two main advantages. First, resonance to electronic transitions provides selectivity in the generation of the cavity modes, allowing all other modes to be silenced by appropriate selection of laser energies. The generation process is thus selective with respect to both the laser and the phonon energies. Second, it avoids terahertz energy limitations intrinsic to metallic layer light-to-sound transducers. The reported experiments give access to the dynamics of the vibrations, enabling studies of the decay times and anharmonicity affecting the cavity modes.

A nanocavity consists of an intermediate layer enclosed by two acoustic Bragg mirrors or superlattices (SLs). Direct generation of sound by femtosecond light pulses in a nanocavity is to be understood in terms of the kind of transducer it provides. Three different mechanisms can lead to the transduction of light pulses into sound: the deformation potential [5], thermal stress [5,6], and photoelastic processes [7]. In the point that follows, we will only consider the third (equivalent conclusions can be surmised if the other mechanisms are regarded). The quantity that determines the transducing properties of the heterostructure is the photoelastic constant p of the different layers. It is strongly dependent on the light energy, being negligible far below the electronic band gap and varying strongly near the gap. If the pump pulse central energy E_L is around the fundamental electronic transition E_{SL} of the SL quantum wells, p will thus result in the profile depicted in Fig. 1(a). Such a quasiperiodic transducer will generate phonon modes with displacement fields u extended throughout the whole heterostructure, as the one shown in the figure. This type of acoustic mode will be referred to as a SL mode, since it does not vary much from the kind of mode into which a perfect SL would transduce a light pulse. On the contrary, a cavity mode presents a displacement field that is maximum in the intermediate cavity layer [1], as shown in Fig. 1(b). To selectively produce such a mode, the transducing properties of the heterostructure need to be enhanced in the cavity layer, as in the photoelastic profile proposed in the lower curve of Fig. 1(b). Such a transducer

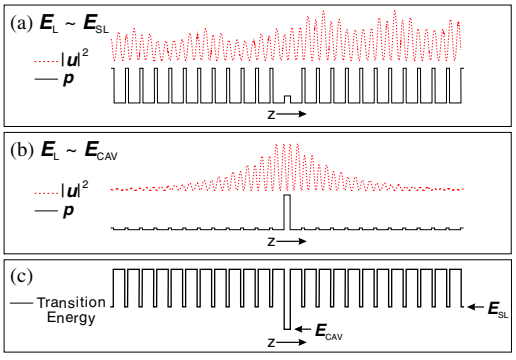

FIG. 1 (color online). (a) Photoelastic constant (p) profile of the sample along an axis z perpendicular to the layers, and typical displacement field u generated when $E_L \sim E_{SL}$. (b) Same as (a) for $E_L \sim E_{CAV}$. (c) Scheme of the fundamental transition energies as a function of the position.

is attained in the present work through a cavity layer that is thicker than the mirror quantum wells. The fundamental transition energy profile of the sample is sketched in Fig. 1(c), where the lowest transition energy corresponds to the cavity layer E_{CAV}. By tuning the laser energy, we are able to turn the transducer from the one in Fig. 1(a), which, as we will show, leads to SL modes, to the one in Fig. 1(b), which generates nanocavity modes. Resonance to electronic transitions has been previously used to excite broadband acoustic pulses selectively in separate quantum wells of different widths [8].

The studied nanocavity consists of two 21 Å/78 Å 12-period $Ga_{0.85}In_{0.15}As/AlAs$ acoustic Bragg mirrors (reflectivity ~99.7%) enclosing a half-wavelength $Ga_{0.85}In_{0.15}As$ spacer (42 Å). The SL unit cell was chosen to maximize the first zone-center minigap around a central frequency of ~0.54 THz [1]. The sample has been previously studied by Raman scattering showing excellent quality [9]. Room temperature photoluminescence (PL) experiments revealed the electronic transitions $E_{CAV} \sim 1.442$ eV and $E_{SL} \sim 1.729$ eV. Reflection-type pump-probe experiments have been performed at room temperature for several laser energies between 1.409 and 1.734 eV. Femtosecond pulses (~ 80 fs) from a mode-locked Ti:sapphire laser, with a repetition rate of 79 MHz, were split into the pump (energy 0.3 nJ) and probe (0.08 nJ) pulses. The pump was modulated at 1.8 MHz by an acousto-optic device in order to allow for synchronous detection. Both pulses were focused onto superimposed ~50 μm-diameter spots.

Figure 2 shows the time evolution of the normalized change of the reflected probe intensity $\Delta R/R$. The signal has been numerically filtered in order to discard electronic decay contributions and Brillouin oscillations. Two laser energies are presented in the figure. For $E_L = 1.722$ eV ~ E_{SL}, two different phenomena are present and at two different time scales. For $t \lesssim 100$ ps, a rapidly vanishing beat is observed [see the detailed region in Fig. 2(b)]. Instead, for $t \gtrsim 100$ ps, a long-living beat remains, constituted only of two main Fourier components ν_1 and ν_2, with $\nu_2 \sim 2\nu_1$. On the other hand, for $E_L = 1.442$ eV ~ E_{CAV}, just the long-living oscillation is present and can be clearly observed in both regions of Fig. 2(b).

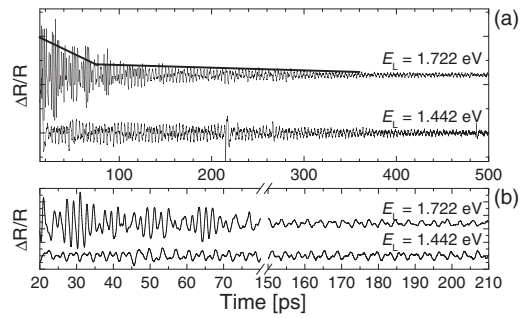

FIG. 2. Normalized reflectivity change of the probe beam as a function of the delay between the pump and the probe for two values of E_L. The data have been numerically filtered with a 0.1-THz-cutoff high-pass Butterworth filter. (a) Full temporal range. The two lines of different slopes indicate two different decay regimes. (b) Expanded regions.

Figure 3(a) shows the Fourier transforms (FT), in the region around the first zone-center minigap, of the time signal for different laser energies. The main feature is the sharp peak at 0.554 THz corresponding to the cavity mode, calculated to appear at 0.54 THz. In addition to it, for high laser energies broad features are also observed. Their amplitude drops off as E_L shifts down from the mirror fundamental transition at 1.729 eV, and they become undetectable at $E_L \sim 1.589$ eV. This dependence on E_L signals that they correspond to SL modes. As a matter of fact, the displacement field in Fig. 1(a) corresponds to the SL peak at 0.588 THz in the top spectrum of Fig. 3(a). It is seen in the experimental data that these SL modes can be *switched off* by detuning E_L from the mirror fundamental transition, allowing for selective generation of the cavity mode.

Let us now focus on the behavior of the cavity mode as E_L varies. Its amplitude oscillates, displaying four local maxima at 1.442, 1.512, 1.631, and 1.710 eV. As follows from PL and photoluminescence excitation (PLE) experiments and envelope function calculations of the electronic levels in the cavity layer quantum well, the first two maxima can be assigned to resonances with the $e1 \rightarrow hh1$ and $e1 \rightarrow lh1$ transitions of the $Ga_{0.85}In_{0.15}As$ cavity layer ($e1$, $hh1$, and $lh1$ are the first confined states of the electron, heavy hole, and light hole, respectively). For the maximum at 1.631 eV, no conclusive evidence of its relation to a specific transition has been found. As regards the maximum at 1.710 eV, it lies in the energy region where the mirrors also absorb, and therefore their contribution should

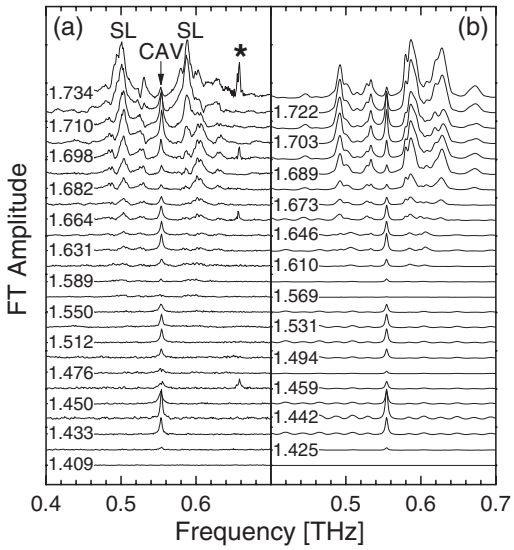

FIG. 3. (a) Fourier transform amplitude of the normalized reflected probe intensity. For each spectrum E_L is expressed in units of eV. CAV and SL indicate the cavity and superlattice modes, respectively. The starred peak is an artifact induced by the laser power stability system. (b) Calculations based on the photoelastic mechanism.

also be taken into account. We will come back to this matter later in the text.

To understand the origin of the features observed in the FT spectra in Fig. 3(a), we need to take into account the generation efficiency as well as the detection response. Previous works have shown that the mechanism which governs the detection in pump-probe experiments is the photoelastic effect [5,6]. It can be proven that the detection response is thus proportional to the Raman backscattering (BS) cross section (see, e.g., [10,11]). Concerning the generation mechanism, we will consider only the photoelastic effect, following the same assumptions made in Ref. [11]. The generation efficiency then turns out to be proportional to the forward scattering (FS) Raman cross section [11]. Non-negligible overlap between FS and BS is assured by finite size effects and light absorption.

In Fig. 4, we show the calculated Raman cross section ranging from the FS spectrum (labeled $k = 0$) to BS typical spectra for the values of E_L used in the pump-probe experiment. The wave vector $\mathbf{k}$ transferred in the Raman process fulfills $\mathbf{k} = \mathbf{k}_L - \mathbf{k}_S$, where $\mathbf{k}_L$ ($\mathbf{k}_S$) is the incident (scattered) photon's wave vector. The FS geometry satisfies $k = 0$, whereas for BS, $k = 2k_L$. The spectra have been calculated according to the photoelastic model [12]. In this figure, we are interested only in the qualitative overall aspect of the Raman spectra, so we have set $p = 1$ within any $Ga_{0.85}In_{0.15}As$ layer and $p = 0$ elsewhere. In the $k = 0$ spectrum, three features are observed. The sharpest peak at 0.554 THz corresponds to the cavity mode. The other two peaks just outside the stop band of the mirrors (gray area) and on either side of it resemble stop-band-edge modes, but they are not exactly such since, due to parity reasons, both stop-band-edge modes are Raman-inactive in the present nanocavity [13]. For small nonvanishing values of k ($kD/\pi = 0.04$–0.08; D is the phonon mirror period), the A_1-type edge mode (0.576 THz) becomes observable,

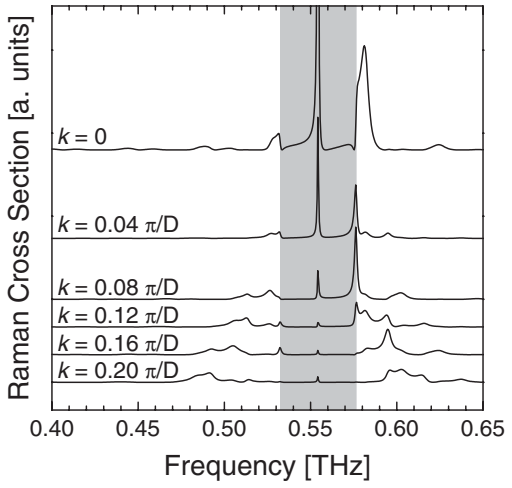

FIG. 4. Calculated Raman spectra for the nanocavity with different values of the transferred wave vector k (D is the acoustic mirror period). $k = 0$ fulfills the FS condition. The gray area covers the mirror stop band.

while the cavity mode intensity falls off, evidencing its zone-center character. For higher values of k, the folded acoustic phonon doublet, modulated by finite size oscillations and interference between the contributions of both mirrors, disperses according to the dispersion relation.

For calculating $\Delta R/R$, the generation is considered proportional to the $k = 0$ Raman spectrum in Fig. 4, whereas for the detection the spectral response is similar to the two lowest curves in the figure, since in the pump-probe experiment E_L covered the interval $0.16 \lesssim kD/\pi \lesssim 0.19$. Some physical constants necessary for the calculations are unknown. For the refractive index, as the optic wavelength is much larger than the SL period, we have considered a continuous optic medium with an effective refractive index $n_{\text{eff}} + i\kappa_{\text{eff}}$, which has been taken as a fitting parameter. The photoelastic properties have been approximated constant within each layer. For AlAs, an arbitrary real value $p_{\text{AlAs}} = 1$ has been fixed. The photoelastic constants of the $Ga_{0.85}In_{0.15}As$ layers in the mirrors (p_{GaInAs}) and of the cavity layer (p_{CAV}) have also been left as fitting parameters. A Lorentzian convolution with a width compatible to the longest delay between the pump and the probe has been included.

The results are plotted in Fig. 3(b). It can be seen that the main features are clearly reproduced: the presence of a cavity mode as well as SL modes on either side of it. By comparison with Fig. 4, it can be seen that the cavity mode and the features at ~0.53 and ~0.59 THz are mainly contributions from the generation efficiency, while the remaining features result from the detection response. The decrease of the SL mode amplitude has been achieved by reducing p_{GaInAs} and κ_{eff} as E_L goes down through E_{SL}. The variation of these parameters has also reproduced the maximum of the cavity mode amplitude at 1.710 eV. In fact, p_{CAV} has been kept at a constant value for $E_L \geq 1.682$ eV. The sensitivity of the cavity mode to the variations of p_{GaInAs} is due to the non-negligible penetration of the mode into the mirrors [see Fig. 1(b)]. For lower laser energies, p_{CAV} has been varied in order to reproduce the cavity mode intensity. The largest value reached was $|p_{\text{CAV}}| = 9.7$, in agreement with the range of values reported in Ref. [14] for various GaAs/AlAs samples. n_{eff} has not shown to introduce significant changes, so it has been fixed to a value of 3.5. The values obtained for the fitting parameters are reasonable. Nevertheless, their interpretation is not straightforward, because they may differ from the real values due to other mechanisms involved in the generation [15]. To account for further details in the spectra, a full calculation of the generated pulse taking into account the different mechanisms should be carried out, but an analysis of the weight of each generation mechanism escapes the scope of this Letter. The simple photoelastic approach has proven able to reproduce the main features in the spectra.

Finally, let us analyze the lifetime of the different acoustic modes. For that, we have computed the FT of the time traces by intervals of 100 ps whose central value scans the

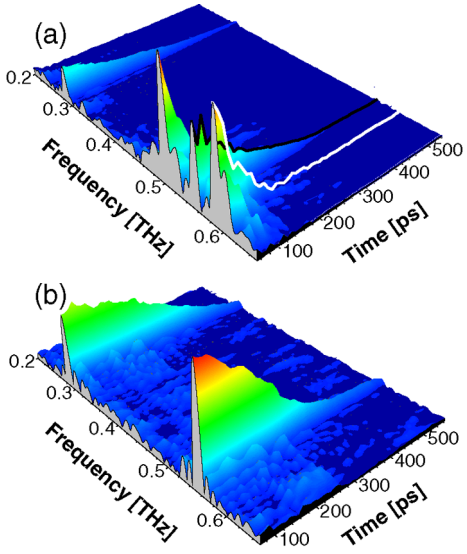

FIG. 5 (color online). Fourier transforms of the time trace by 100-ps intervals. The time axis indicates the center of the intervals. (a) $E_L = 1.710$ eV. The black (white) line follows the decay of the cavity mode (a SL mode). (b) $E_L = 1.442$ eV.

whole time range. The results are presented for $E_L = 1.710$ eV in Fig. 5(a) and 1.442 eV in Fig. 5(b). In Fig. 5(a), the cavity and SL modes are clearly recognized between 0.46 and 0.64 THz. Another mode is also observed at 0.285 THz. It is a lower energy cavity mode corresponding to the first zone-edge minigap, having approximately half the frequency of the other cavity mode. The combination of both cavity modes results in the two-frequency beat observed in Fig. 2. In Fig. 5(b), it is seen that, when E_L is resonant to the cavity layer fundamental transition, only the cavity modes are selectively generated. It is clear in the figure that the lower mode lives longer than the higher. Although the decaying shape is not perfectly exponential, we estimate a decay time τ_{exp} as the time it takes each mode to reduce its amplitude by a factor $1/e$. The obtained values are (350 ± 10) and (210 ± 6) ps for the lower and higher modes, respectively. In the case of the lower mode, τ_{exp} matches rather well the decay time τ_{conf} due to confinement $\tau_{conf} = (290 \pm 40)$ ps, calculated as the inverse of the full width at half maximum of the lower cavity mode in the theoretical acoustic transmissivity spectrum. On the contrary, whereas the cavity is optimized for the higher mode, this one presents a shorter τ_{exp} than the lower mode, and it is also much shorter than the expected value $\tau_{conf} = (710 \pm 10)$ ps. We therefore conclude that at high energies the decay time is strongly affected by anharmonic processes. If a relation $\tau_{exp}^{-1} = \tau_{conf}^{-1} + \tau_{anh}^{-1}$ is assumed, where τ_{anh} is the decay time due to anharmonicity, the returned value is $\tau_{anh} = (300 \pm 10)$ ps. Energy interconversion between the two cavity modes makes a plausible explanation for the differences between τ_{exp} and τ_{conf} seen in both modes, but further verification would be needed. To fully test the confinement properties of the cavity, a systematic study of the cavity mode lifetime as a function of temperature would be of great interest. As regards the SL modes, it is observed in Fig. 5(a) that none of them lives longer than the higher cavity mode. The value of τ_{exp} for the SL mode at 0.603 THz, for example, is (37 ± 3) ps. The SL modes escape rapidly towards the substrate with a velocity determined by the dispersion relation. A calculated escape time of (44 ± 2) ps matches rather well τ_{exp}, which is too short to render anharmonic effects evident. While the SL modes escape to the substrate, the longer decay time of the cavity modes manifests the confinement properties [4]. The phonon oscillates back and forth in the cavity, and it slowly tunnels through to the substrate. For the higher mode, the number of oscillations is, however, limited by anharmonic decay, and we estimate it to (8.5 ± 0.4) [16].

In summary, we have demonstrated selective generation of coherent acoustic nanocavity modes. The selectivity is attained by tuning the incident pulse energy to the cavity spacer electronic transitions. The photoelastic model has been able to explain the main features in the experimental spectra, although other generation mechanisms cannot be discarded. The decay time of the modes has been analyzed as well. We have found significantly longer decay times for the cavity modes, evidencing the confinement effect. Anharmonic effects have also proven to be involved in the decay of the higher energy cavity mode.

We thank K. Meunier for the PLE experiments. M. F. P. W. acknowledges the program Alβan, the European Union Programme of High Level Scholarships for Latin America, Grant No. E05D051993AR. Support from SECyT-ECOS and the ONR (A. F.) is also acknowledged.

*afains@cab.cnea.gov.ar
†Present address: ATR Laboratories, Sharp Corporation, 2613-1, Ichinomoto, Tenri, Nara 632-8567, Japan.

[1] M. Trigo *et al.*, Phys. Rev. Lett. **89**, 227402 (2002).
[2] A. Bartels *et al.*, Appl. Phys. Lett. **72**, 2844 (1998); C.-K. Sun *et al.*, Appl. Phys. Lett. **78**, 1201 (2001).
[3] A. J. Kent *et al.*, Phys. Rev. Lett. **96**, 215504 (2006).
[4] A. Huynh *et al.*, Phys. Rev. Lett. **97**, 115502 (2006).
[5] C. Thomsen *et al.*, Phys. Rev. B **34**, 4129 (1986).
[6] O. Matsuda *et al.*, J. Opt. Soc. Am. B **19**, 3028 (2002).
[7] R. Merlin, Solid State Commun. **102**, 207 (1997).
[8] O. Matsuda *et al.*, Physica (Amsterdam) **316B–317B**, 205 (2002).
[9] G. Rozas *et al.*, Phys. Rev. B **72**, 035331 (2005).
[10] K. Mizoguchi *et al.*, Phys. Rev. B **60**, 8262 (1999).
[11] N. D. Lanzillotti Kimura *et al.*, Phys. Rev. B **71**, 041305(R) (2005).
[12] B. Jusserand and M. Cardona, in *Light Scattering in Solids V*, edited by M. Cardona and G. Güntherodt (Springer, Heidelberg, 1989), p. 49.
[13] M. F. Pascual Winter *et al.* (to be published).
[14] J. Sapriel *et al.*, Phys. Rev. B **37**, 4099 (1988).
[15] T. E. Stevens *et al.*, Phys. Rev. B **65**, 144304 (2002).
[16] P. Lacharmoise *et al.*, Appl. Phys. Lett. **84**, 3274 (2004).